

Scanned Image Data from 3D-Printed Specimens Using Fused Deposition Modeling

Felix W. Baumann *, Julian R. Eichhoff and Dieter Roller

Institute of Computer-aided Product Development Systems, University of Stuttgart, 70569 Stuttgart, Germany; julian.eichhoff@informatik.uni-stuttgart.de (J.R.E.); roller@informatik.uni-stuttgart.de (D.R.)

* Correspondence: baumann@informatik.uni-stuttgart.de; Tel.: +49-711-685-88315

Academic Editor: Jamal Jokar Arsanjani

Received: 11 October 2016; Accepted: 22 December 2016; Published: 1 January 2017

Abstract: This dataset provides high-resolution 2D scans of 3D printed test objects (dog-bone), derived from EN ISO 527-2:2012. The specimens are scanned in resolutions from 600 dpi to 4800 dpi utilising a Konica-Minolta bizHub 42 and Canon LiDE 210 scanner. The specimens are created to research the influence of the infill-pattern orientation; The print orientation on the geometrical fidelity and the structural strength. The specimens are printed on a *MakerBot Replicator 2X* 3D-printer using yellow (ABS 1.75 mm Yellow, REC, Moscow, Russia) and purple ABS plastic (ABS 1.75 mm Pink Lion&Fox, Hamburg, Germany). The dataset consists of at least one scan per specimen with the measured dimensional characteristics. For this, software is created and described within this work. Specimens from this dataset are either scanned on blank white paper or on white paper with blue millimetre marking. The printing experiment contains a number of failed prints. Specimens that did not fulfil the expected geometry are scanned separately and are of lower quality due to the inability to scan objects with a non-flat surface. For a number of specimens printed sensor data is acquired during the printing process. This dataset consists of 193 specimen scans in PNG format of 127 objects with unadjusted raw graphical data and a corresponding, annotated post-processed image. Annotated data includes the detected object, its geometrical characteristics and file information. Computer extracted geometrical information is supplied for the images where automated geometrical feature extraction is possible.

Data Set: <http://doi.org/10.5281/zenodo.159676>

Data Set License: CC-BY

Keywords: image scan; geometrical analysis; 3D printing; fused deposition modeling

1. Introduction

Additive Manufacturing (AM) or 3D printing [1] is the method of creating physical objects from digital models by usually layer-wise fabrication. This term comprises various technologies used to create the physical objects [2,3] ranging from Laminated Object Manufacturing (LOM), Selective Laser Sintering (SLS) or Selective Laser Melting (SLM), Stereolithography (SLA) to Fused Deposition Modeling (FDM) (or Fused Filament Fabrication (FFF) [4]). Objects can be created using a range of materials like plastics (Thermoplastics or Photopolymers), Ceramics, Waxes, Metals and Alloys dependent upon the underlying technology. Due to the nature of the fabrication process the digital Computer Aided Design (CAD) model must be transformed to a machine code file [5]. For this step the digital model is transformed into an exchange format like StereoLithography (file format) (STL) or Additive Manufacturing File Format (AMF) [6] which is then processed by a software that is called a slicer. The slicing software creates layers or cross-sections through the object under the influence

of user-selectable parameters that is then traced by the machine-code. The quality of the resulting object is dependent upon the quality of the slicer [7]. In FDM [8] a thermoplastic like acrylonitrile butadiene styrene (ABS) polylactic acid (PLA) is heated to above the glass-transition temperature within the extruder to a semi-molten state and then pushed onto the build plate or previous layers of the printed object, where the extrudate solidifies due to the reduced temperature [9]. This research is conducted to test the hypotheses that the build orientation and the infill pattern of a part influence the mechanical and geometrical (see Section 1.1) properties of said part. For this research we have created a set of infill patterns ranging from 0 to 90 degrees (0, 5, 10, 30, 45, 60 and 90 degrees, see Figure 1), where the angle indicates the orientation of the strands within the specimen against the X-axis which is the front of the build plate, see Figure 1. The experiment is designed to print the varying infill patterns with and without orientation of the object in alignment of the infill pattern. The specimens are printed with a layer height of 0.3 mm and a two layer design. The second layer is oriented either identical to the first layer or mirrored to the first layer. For this experiment the following four groups are created for each of the infill patterns:

- Aligned, Mirrored second layer (flip)
- Aligned, Identical second layer (norm)
- Not Aligned (orient), Mirrored second layer (flip)
- Not Aligned (orient), Identical second layer (norm)

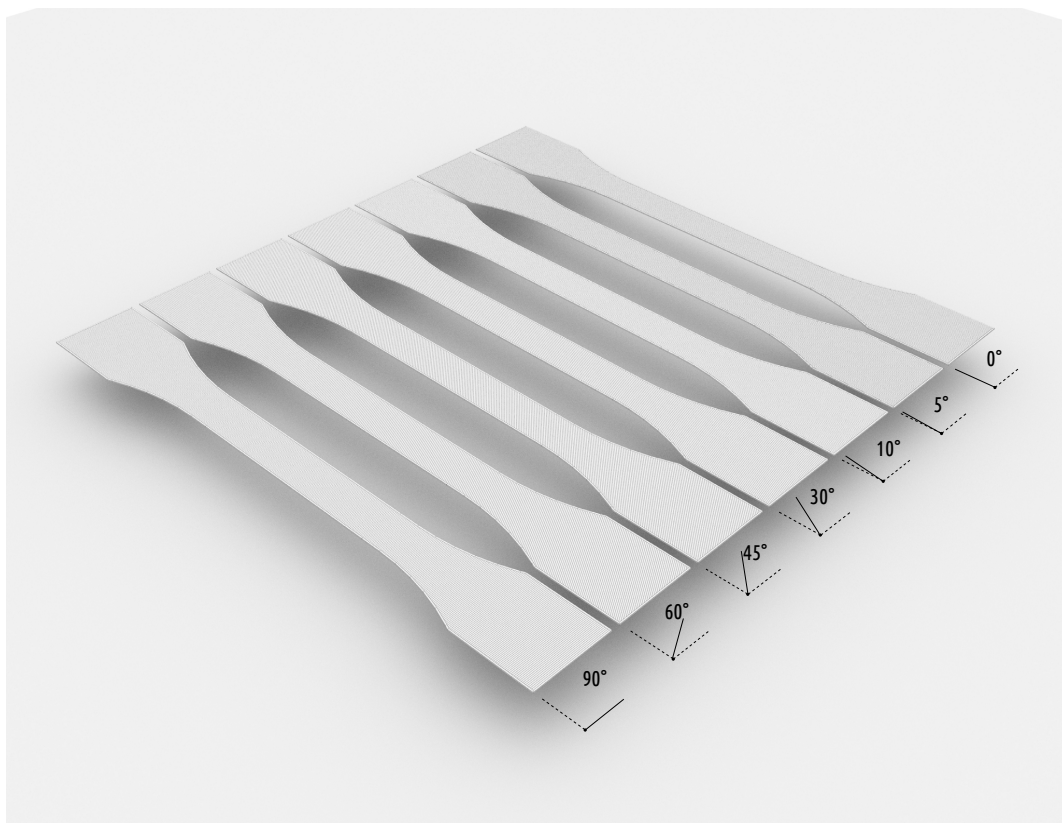


Figure 1. Overview of infill patterns used in experiment, image courtesy of David Correa.

In the Figures 2 and 3 the placement of the specimen on the printing bed is displayed. In Figure 2 a specimen with a 45 degree infill pattern is displayed – the infill pattern is indicated by the red stripes within the specimen. This specimen is rotated at 45 degrees against the X-axis of the printer. The infill pattern is oriented along the Y-axis of the 3D-printer. In Figure 3 the specimen with the same 45 degree infill pattern is depicted. In this configuration, the specimen is aligned with its longest side

to the X-axis of the 3D-printer. In this case the infill pattern is not aligned with either the X-axis or the Y-axis.

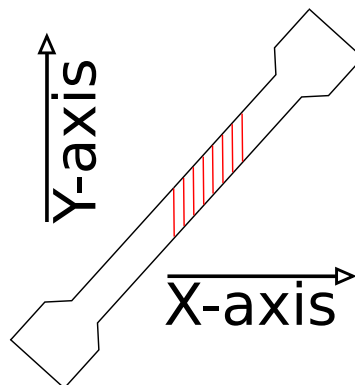


Figure 2. Specimen with 45 degree infill pattern in rotated position on the printing bed.

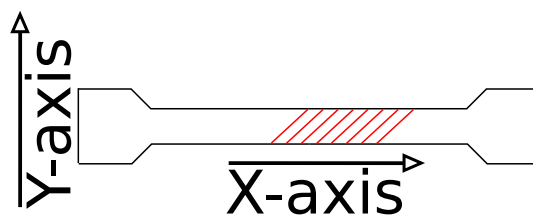


Figure 3. Specimen with 45 degree infill pattern in oriented position on the printing bed.

Further experiments are conducted on the sensor data acquisition during the printing process for state detection [10], for which the 3D printer (*Makerbot Replicator 2X*) is equipped with sensor nodes registering ambient (e.g., temperature, air pressure and magnetic fields) and inherent data (e.g., vibration).

For the seven infill patterns and a minimum of 3 prints per group this yields an expected sample size of: $7 \times 4 \times 3 = 84$. The experiment found that some models resulted in misprints and flawed objects that are partially unscannable (especially infill pattern 5 and 10 degrees). For a full coverage the following objects are missing:

- 1 × 45 degrees norm orient, omitted due to machine error
- 3 × 10 degrees flip orient, printed but of unusable quality due to printing errors

1.1. Accuracy

The accuracy and geometrical fidelity of 3D-printed objects is researched in many works and for over 20 years [11,12] due to the necessity to produce objects that match their digital models closely for the use as prototypes (Rapid Prototyping, (RP) [13,14]), consumer products (Rapid Manufacturing, (RM) [15]) or tools (Rapid Tooling, (RT) [16]).

Dimitrov et al. [17] conducted a study on the accuracy of the Powder bed and inkjet head 3D printing (3DP) process with a benchmark model. Among the three influencing factors for the accuracy is the selected axis and the material involved.

Turner and Gold [18] provide a review on Fused Deposition Modeling (FDM) with a discussion on the available process parameters and the resulting accuracy and resolution.

Boschetto and Bottini [19] develop a geometrical model for the prediction of the accuracy in the Fused Deposition Modeling (FDM) process. They predict the accuracy based on process parameters for a case study for 92% of their specimens within 0.1 mm. Armillotta [20] discusses the surface quality of Fused Deposition Modeling (FDM) printed objects. The author utilises a non-contacting

scanner with a resolution of 0.03 mm for the assessment of the surface quality. Furthermore, the work delivers a set of guidelines for the FDM process in respect to the achievable surface quality.

Equabal et al. [21] present a Fuzzy classifier and neural-net implementations for the prediction of the accuracy within the Fused Deposition Modeling (FDM) process under varying process parameters. They achieve a mean absolute relative error of 5.5% for the predictor based on Fuzzy logic.

Sahu et al. [22] also predict the precision of FDM manufactured parts using a Fuzzy prediction, but with different input parameters (Signal to noise ratio of the width, length and height).

Katatny et al. [23] present a study on the dimensional accuracy of Fused Deposition Modeling (FDM) manufactured objects for the use as medical models. The authors captured the geometrical data with a 3D Laser scanner at a resolution of 0.2 mm in the vertical direction. In this work a standard deviation of 0.177 mm is calculated for a model of a mandible acquired from Computer Tomography (CT) data.

To counter expected deviations of the object to the model, Tong et al. [24] propose the adaption of slice files. For this adaption the authors present a mathematical error model for the Fused Deposition Modeling (FDM) process and compare the adaption of slice files to the adaption of Stereolithography (file format) (STL) files. Due to machine restrictions the corrections in either the slice file and the Stereolithography (file format) (STL) file are comparable, i.e., control accuracy of the 3D-printer is not sufficient to distinguish between the two correction methods.

Boschetto and Bottini [25] discuss the implications of Additive Manufacturing (AM) methods on the process of design. For this discussion they utilise digitally acquired images to compare to model files.

Garg et al. [26] present a study on the comparison of surface roughness of chemically treated and untreated specimens manufactured using FDM. They conclude that for minimal dimensional deviation from the model the objects should be manufactured either parallel or perpendicular to the main axis of the part and the 3D-printer axis.

From the literature the following taxonomy (Table 1 can be constructed, based on the utilized techniques for accuracy measurement and applicability restrictions or generalisations. From the literature it is evident, that either manual measurements, optical analysis, 3D laser-scanning or coordinate measuring machines are applied for the geometrical analysis of 3D-printed objects. Methods to assess the surface roughness of 3D-printed objects are specific to the applied technology, as the traces of the manufacturing are expressed significantly different for each technology. For example, with Fused Deposition Modeling (FDM) manufacturing, the object is created by extruding filament bead-wise along the machine-path thus leaving bead-like artefacts on the surface. With Selective Laser Melting (SLM), an object manufactured does not express such bead-like structures, as the material gets molten by the laser in a different pattern, with partial remelting of previous material.

Table 1. Taxonomy of Accuracy Measurement in Literature.

Source	Achieved Accuracy	Applied for	Applicable for	Restriction(s)	Type
[21]	0.01 mm	Fused Deposition Modeling (FDM)	3D-objects	None	Manual – Using <i>Mitutoyo</i> [27] Vernier Calliper
[22]	0.01 mm	FDM	3D-objects	None	Manual – Using <i>Mitutoyo</i> [27] Vernier Calliper
[19]	16 nm	FDM	Surface profile of planar 3D-objects	FDM	Manual – Using <i>Taylor Hobson Form Talyprofile Plus</i> [28] Image processing – <i>Canon Canoscan Lide 90</i> [29] 1200 dpi, and manual measurement with <i>Borletti MEL/N 2W</i> [30] micrometer
[25]	0.22 mm	FDM	3D-objects with planar surface	None	Theoretical, Review
[18]	N/A	None	Various	None	Laser-Scanning – Using <i>Roland LPX-250</i> [31]
[23]	0.2 mm	FDM	3D-objects	None	<i>Carl Zeiss ECLIPSE 550 CMM</i> [32]
[24]	N/A	FDM+ Stereolithography (SLA)	3D-objects	None	Manual – Using <i>Mitutoyo SJ400</i> [27] for surface roughness, dimensions with <i>Nikon V-10A</i> [33]
[26]	0.001 mm	FDM+ surface treatment	3D-objects	None	

Table 2. Average Image Properties for the Varying Resolutions.

dpi	Max. Equivalent of 1 Pixel (px) in mm	Number of Available Images	Avg. Filesize in MiB	Average Image Width in Pixel (px)	Average Image Height in Pixel (px)
600	0.0423333	17	47.0928	4997.4705	5410.8235
1200	0.0211666	21	180.3056	10,224.0000	10,893.2857
2400	0.0105833	19	688.6836	20,464.0000	21,943.4736
4800	0.0052916	13	1323.7478	40,944.0000	45,268.6153

2. Materials and Methods

The image data acquisition is performed using a *Konica Minolta BizHub 42* and a *Canon LiDE 210* scanner. The *BizHub* is capable of producing lossless images up to a resolution of 600 dpi (also pixels (px) per Inch) as Tagged Image File Format (TIFF) [https://partners.adobe.com/public/developer/en/tiff/TIFF6.pdf] files. The *LiDE 210* device is capable of producing images up to a resolution of 4800 dpi in a format depending upon the acquisition software (Tagged Image File Format (TIFF) is used in this experiment). With these resolutions available, the image size, average file size (for the Portable Network Graphics (File Format) (PNG) format see [34]) and the theoretical maximum resolution is listed in Table 2. The theoretical maximum resolution is calculated by:

$$1\text{px} = \frac{2.54}{\text{dpi}} \times 10 \text{ mm} \quad (1)$$

The specimens are scanned on either blank white paper or paper with blue millimetre marking affixed with scotch tape to prevent misalignment during the scanning procedure. The image data, see Figure 4, is then cropped for the individual specimens using GNU Image Manipulation Program (*GIMP*) as an image manipulation tool (Version 2.8.16).

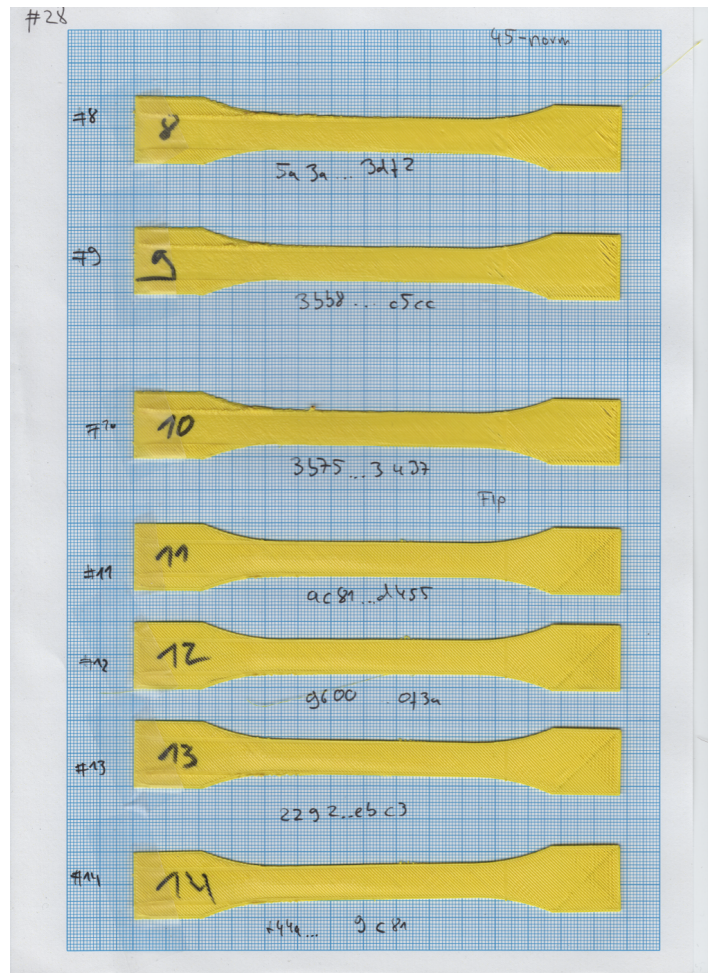


Figure 4. Uncropped and unaltered raw image data acquired with Canon LiDE 210 at 1200 dpi containing specimens 8, 9, 10, 11, 12, 13 and 14 from page 28, filesize is 431.1 MiB in Tagged Image File Format (TIFF) format. Image dimensions are 10,224 pixel (px) in width and 14,055 pixel (px) in height. Image is converted to Portable Network Graphics (File Format) (PNG) for display within this document. Image is scaled to 1024 pixel (px) width for display.

The individual specimen image data is then stored as Tagged Image File Format (TIFF) file format with Lempel-Ziv-Welch (Algorithm) (LZW) compression [35] for smaller file sizes, see Figure 5.

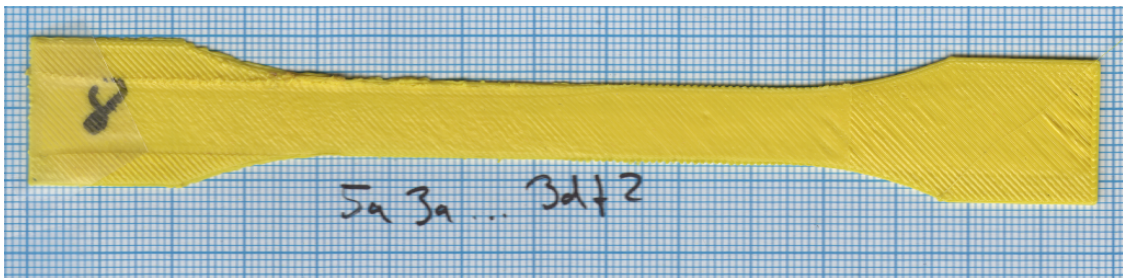


Figure 5. Cropped specimen (8) stored in Tagged Image File Format (TIFF) file format with Lempel-Ziv-Welch (Algorithm) (LZW) compression at 1200 dpi, filesize is 26.3 MiB. Image size is 7360 pixel (px) in width and 1794 pixel (px) in height. Image is converted to Portable Network Graphics (File Format) (PNG) for display within this document. Image is scaled to 1024 pixel (px) width for display.

In the following step the Tagged Image File Format (TIFF) image is converted into the lossless Portable Network Graphics (File Format) (PNG) format using *imagemagick* (Version 6.9.3-0) and optimised using *optipng* (Version 0.7.5, parameters used “-fix -o 5”) for further reduction in filesize.

The software to extract the geometrical information from the scanned data is written in *Python* (Version 2.7.11) using the *OpenCV* framework (Version 2.4.12.2) for image processing. The algorithm to extract the geometrical information is described as follows:

1. Crop the original form to contain each individual printed object
2. Foreach cropped area of interest around the object do
 - (a) Transform the Red-Green-Blue (Color Coding) (RGB) image data to Hue-Saturation-Value (Color Coding) (HSV) for more resistant colour based object detection
 - (b) Identify image background and measurement mesh (static) and subtract from image
 - (c) Binarize image by thresholding with most common colour in image
 - (d) Utilise *OpenCV* blob detection algorithm on result and select largest blob as candidate for object detection
 - (e) Detect corners of object detection candidate and transform to array of line segments
 - (f) Close holes within the maximum border segment
 - (g) Create bounding-box around candidate object and compare to expected result
 - i. if object candidate is verified then:
 - ii. Scan left side for corner top-left (Point A)
 - iii. Scan left side for corner bottom-left (Point B)
 - iv. Scan right side for corner top-right (Point C)
 - v. Scan right side for corner bottom-right (Point D)
 - vi. Calculate distance between Point A and Point C (Distance Top) and angle against horizontal for AC
 - vii. Calculate distance between Point B and D (Distance Bottom) and angle against horizontal for BD
 - viii. Calculate distance between Point A and B (Distance Left) and angle against horizontal for AB
 - ix. Calculate distance between Point C and D (Distance Right) and angle against horizontal for CD
 - x. Determine average X position of upper border near object centre
 - xi. Determine average X position of lower border near object center
 - xii. Calculate Average distance between upper and lower border near object centre (Middle Width)
 - xiii. Calculate area surrounded by detected border divided by area of bounding box

- (h) Create overlay information for original image (intended for human usage)
- (i) Store data in database for later retrieval

For the corner detection two approaches are used as the specimens and are not equipped with accurate corners, but rounded corners due to the nature of the manufacturing technique. The first corner detection utilizes extensions of the vertical and horizontal borders and defines the corner as the intersection of these, see Corner A in Figure 6. The second approach is to detect the nearest point on the outline of the specimen to the respective corner of the image frame, e.g., the top-left corner of the specimen is the point on the outline of the specimen that is closest to the top-left corner of the image (Position $X = 0$ and $Y = 0$), see Corner B in Figure 6.

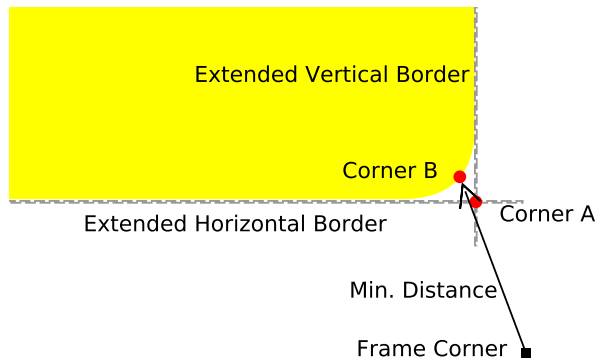


Figure 6. Schematic view of corner detection.

The significant points and measurement identifiers are depicted in Figure 7.

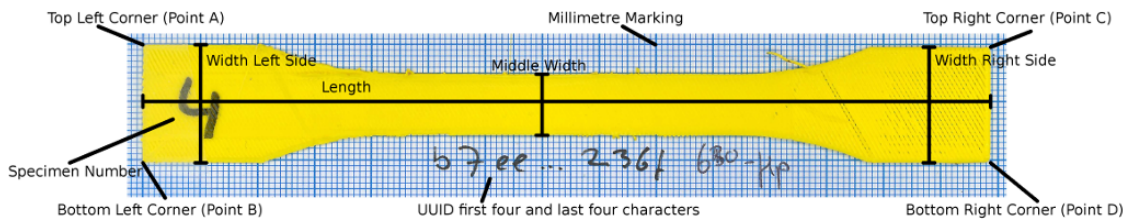


Figure 7. Description of significant point within the scanned image data for reference - Specimen 4 depicted. Image is scaled to 1024 pixel (px) width for display.

An overlay enriched image is created by the software that includes information on the filename, the measured distances (length of object measured from the top corners and along the longest axis of the object; width of object at the left and right side; width of the object in the middle), its orientation, the angle of the enclosing ellipse and the deduced infill pattern in degrees. Furthermore, this overlay image highlights the detected object and places a bounding box as well as a box through the corners of the object as an overlay. Further information is extracted and stored in a text file where each line is associated with a datum. These data are described in Section 3. See Figure 8 for an example of the result of the software processing with the overlaid information on the original image data.

The experiment uses a model derived from EN ISO 527-2:2012 [36] for structural testing of plastic based specimen with the deviation of object thickness that is reduced to 2 layers of 0.3 mm each. See Figure 9 for a reference of the object geometry. The unprocessed image data is provided as an example in Figure 10 for specimen 50.

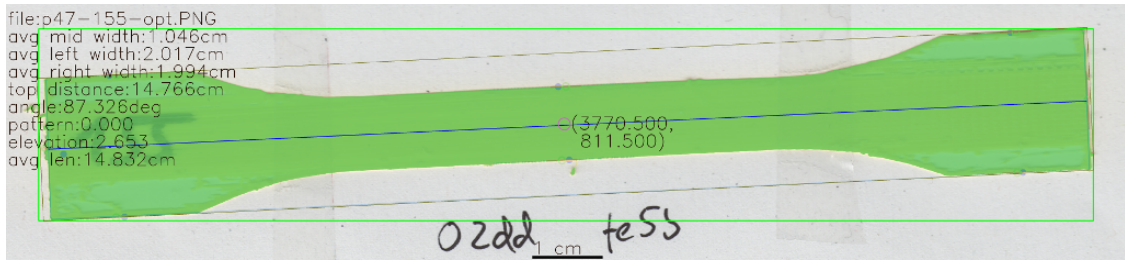


Figure 8. Overlay image data for specimen 155 as a result from the software processing. Image in Portable Network Graphics (File Format) (PNG) format with a filesize of 11.5 MiB and image dimensions of 7535 px width and 1716 px height. Image is scaled to 1024 px width for display.

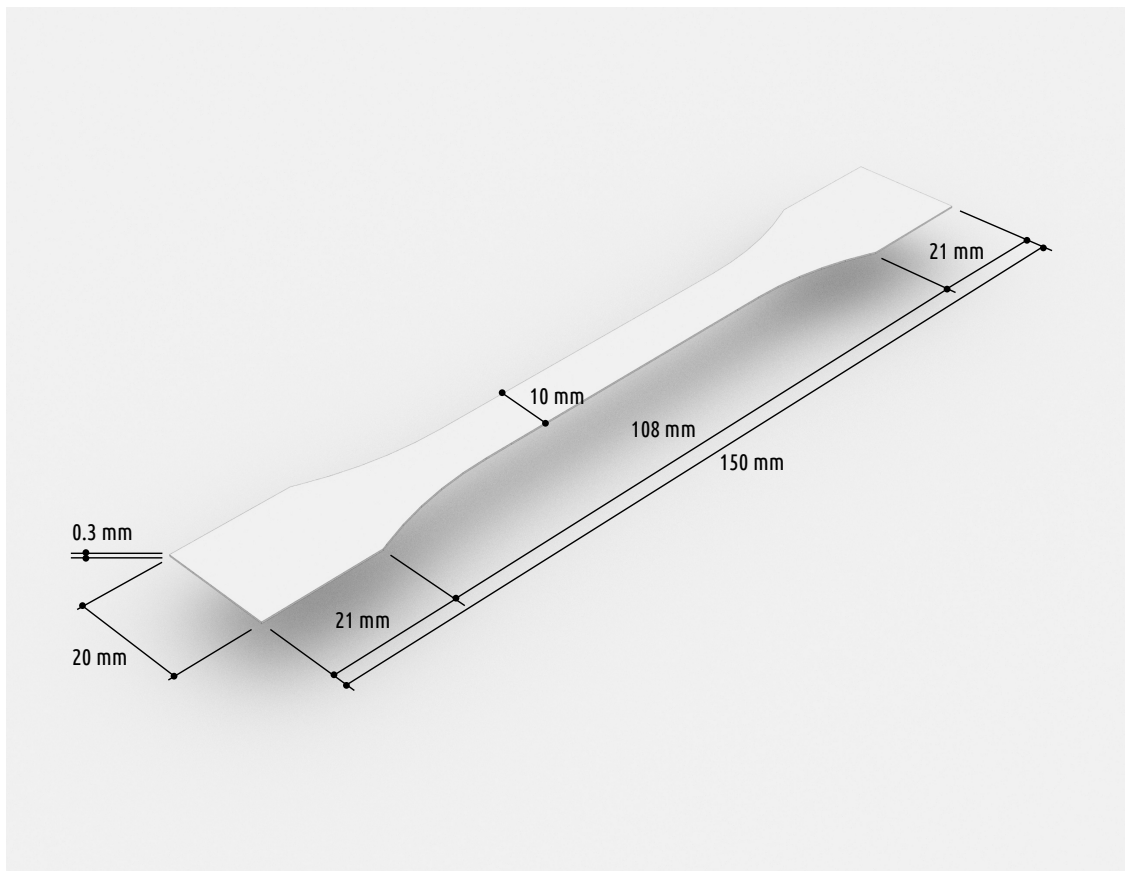


Figure 9. Object dimensions for one layer, image courtesy of David Correa.



Figure 10. Cropped scanned image data for specimen 50 on paper with blue millimetre marking. Image is scaled to 1024 pixel (px) width for display.

Although the experiment is conducted on flat, single and dual layer specimens – which are not representative of real-world objects – it displays erroneous and expected behaviour in the deposition

of thermoplastic material. The material deposition structure is governed by the choice of material, the selection of parameters for the execution and the quality of the 3D-printer in use. The dataset is generated from an experiment on (to published separately) the structural stability of various infill patterns and build orientation which evaluates flexural stress for FDM printed specimens using acrylonitrile butadiene styrene (ABS) plastics. In combination with this analysis the dataset can help to research the relationship between visually apparent structures and stress quality of objects. The data can also be used to visually analyse patterns and structures indicating flawed execution to ascertain the quality of the executing 3D-printer and develop more accurate models of deposition strategies. From the visual data analysis systematic shrinkage can be researched under the influence of the varying infill patterns. For the analysis on the impact of the infill and build orientation on the geometrical fidelity, we refer to the publication by Baumann et al. [37]. Furthermore, the scanned image based and software supported geometrical analysis of the specimen is applicable for the rapid measurement of specimens for testing according to the EN ISO 527-2:2012 [36] standard.

2.1. Error Estimation

From the theoretical px lengths for each of the resolutions provided in the Table 3 below the following error estimation for the proposed and applied method can be derived.

Table 3. Measured Errors for references in various resolutions.

dpi	max	min	pos. diff	neg. diff	pos. diff %	neg. diff %	pos. diff real	neg. diff real
600	246	228	9.78	−8.22	4.14 %	3.48 %	0.41 mm	−0.35 mm
1200	493	458	20.56	−14.44	4.35 %	3.06 %	0.44 mm	−0.31 mm
2400	984	917	39.12	−27.88	4.14 %	−2.95 %	0.41 mm	−0.30 mm
4800	1952	1827	62.21	−62.79	3.29 %	−3.32 %	0.33 mm	−0.33 mm

In Figure 11 an example for this error measurement is depicted. In this figure, the reference lines are analysed with the *GIMP* software. The dotted lines are from the software. The pixels from the reference lines are not sharp and lead to measurement errors. Such measurement errors do also occur on the corners and borders of the specimen.

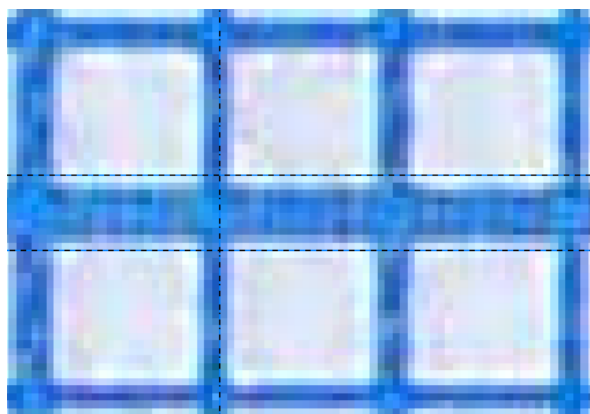


Figure 11. Measurement uncertainty apparent in GIMP for line thickness analysis.

As the pixels (pxs) in the digital image tend to bleed and the contours of the features are unsharp, an uncertainty for the measurements is inherent. To calculate the uncertainty of the method, measurements are taken to estimate known distances of 1 cm and 5 mm. The measurements are taken at two positions with the first position being placed above the actual feature so that this reflects the maximum distance. The second position is taken below the feature so that this measurement reflects the minimum distance. The measurements are then compared to the theoretical values for these

distances as listed in Table 3, third column. In this column the pixels (pxs) for a distance of 1 cm are listed for the respective resolution.

In Table 4 the equivalencies for the digital units, i.e., px, to the real world units, i.e., mm and cm, respectively, are listed. The second column indicates the equivalent of 1 px in mm and the third column indicates the equivalent of 1 cm in pixels (pxs).

Table 4. Equivalencies of digital and real world units for different resolutions.

	1 px equiv. \times mm	1 cm equiv. \times px
600	0.0423333	236.22
1200	0.0211666	472.44
2400	0.0105833	944.88
4800	0.0052916	1889.79

In Table 3 the following abbreviations for the columns are in use:

- **max** and **min** for the maximum and minimum measured distances for the 1 cm reference in pixels (pxs)
- **pos. diff** and **neg. diff** for the positive and negative difference to the theoretical value for the reference distance as indicated in Table 4.
- **pos. diff %** and **neg. diff %** for the percentage difference of the differences to the theoretical values
- **pos. diff real** and **neg. diff real** for the real-world differences in mm to the theoretical value.

In Table 5 the average percentage and real errors for the averaged measurements of the reference length are listed per resolution.

Table 5. Average Errors for references in various resolutions.

dpi	Average	diff	diff %	diff Real
600	237.0	0.78	0.33 %	0.033 mm
1200	475.5	3.06	0.65 %	0.065 mm
2400	950.5	5.62	0.59 %	0.059 mm
4800	1889.5	−0.29	0.02 %	0.002 mm

2.2. On the Data Acquisition Device and Data Acquisition

The image data is acquired using a *Canon LiDE 210* optical flatbed scanner for which the specification is available at <https://www.usa.canon.com/internet/portal/us/home/support/details/scanners/photo-scanner/canoscan-lide-210>. This scanner has an optical resolution of 4800×4800 dpi and offers an interpolation mode of up to $19,200 \times 19,200$ dpi. Only optically available resolutions are used for the data acquisition. The scanning unit moves from the front of the device to the backside of the device. The front of the device is identified by the location of the interface-buttons. In the experiment this translates to a movement from the top of the scanned page to the bottom. The scanning unit has an integrated light source below the contact image sensor (CIS) leading to a narrow shadow line above the scanned objects, see Figure 12 for a schematic view of the scanning device and the specimens placement. Automatic image enhancement techniques and filters are disabled for the scanning procedure.

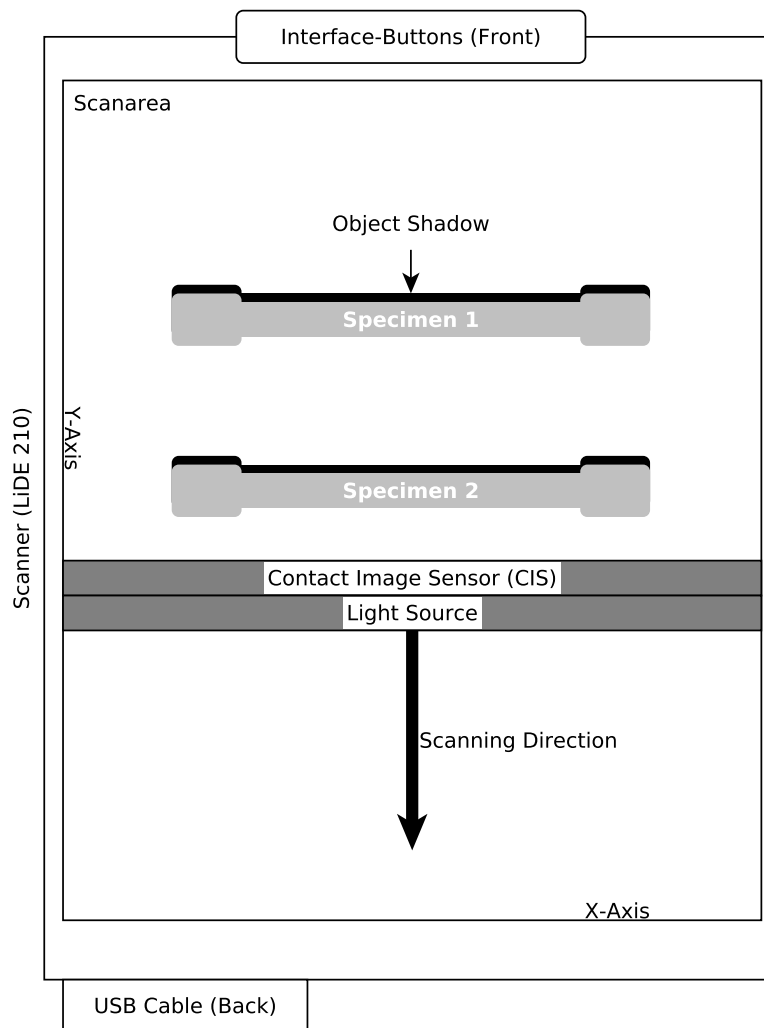


Figure 12. Schematic view of the scanning device and specimens placement.

3. Dataset Description

The dataset is split into four parts:

- Part A, contains the original scanned A4 papers with the specimens affixed.
- Part B, contains the cropped and extracted, unaltered scanned data for each individual specimen.
- Part C, contains the augmented image data for each individual specimen as provided by the analysis software.
- Part D, contains the data files for each individual specimen as provided by the analysis software.

The files are identified following the schema:

$$p\langle\text{PAGE_NUM}\rangle\text{-}\langle\text{SPECIMEN_NUM}\rangle\text{-}\langle\text{RES}\rangle.\langle\text{FILE_TYPE}\rangle \quad (2)$$

where PAGE_NUM indicates the page identifier this specimen is placed on, SPECIMEN_NUM indicates the individual specimens number, and FILE_TYPE indicates whether this is an image (indicated by PNG) or a data file (indicated by LOG). RES indicates the respective resolution in DPI

and can be either 600, 1200, 2400 or 4800. Data from part C is following a different naming schema to distinguish the augmented and raw image data. Image data in part C is named:

$$p\langle\text{PAGE_NUM}\rangle-\langle\text{SPECIMEN_NUM}\rangle\text{-opt-res.PNG} \quad (3)$$

The geometrical data extracted from the image data files and stored in the respective data files is described as follows. Each line of also contains an example output from the analysis software for specimen 67.

1. Width - Width of the scanned image in pixel (px) (7440)
2. Height - Height of the scanned image in pixel (px) (1648)
3. h - Colour Hue in the Hue-Saturation-Value (Color Coding) (HSV) Colourspace of the most dominant colour (25)
4. s - Colour Saturation in the HSV Colourspace of the most dominant colour (165)
5. v - Colour Value in the HSV Colourspace of the most dominant colour (247)
6. r - Colour Value Red-Channel in the Red-Green-Blue (Color Coding) (RGB) Colourspace of the most dominant colour (88)
7. g - Colour Value Green-Channel in the RGB Colourspace of the most dominant colour (218)
8. b - Colour Value Blue-Channel in the RGB Colourspace of the most dominant colour (247)
9. cm_factor - Factor to calculate from pixels to cm (236.22047)
10. tmp_area - Largest found area for further detection (4908256.00000)
11. calc_dist_right_side - Calculated distance at the right side (width) in pixel (px) (984.67546)
12. calc_dist_right_side_cm - Calculated distance at the right side (width) in cm (2.08423)
13. avg_right_side_A_x - Average X position for point A for the distance calculation (6718.12857)
14. avg_right_side_A_Y - Average Y position for point A for the distance calculation (1122.64286)
15. avg_right_side_B_X - Average Y position for point B for the distance calculation (6722.41860)
16. avg_right_side_B_Y - Average Y position for point B for the distance calculation (137.97674)
17. line_1_right_side - Definition of a line through the positions of elements detected on the border of the right top side in the form of $f(x) = K \times x + l$. Gradient and y-intercept (-0.04906 + 1452.20479)
18. line_2_right_side - Definition of a line through the positions of elements detected on the border of the right bottom side in the form of $f(x) = K \times x + l$. Gradient and y-intercept (-0.04322 + 428.53713)
19. distA_right_side - Calculated distance of a line perpendicular to the line_1_right_side and its intersection of line_2_right_side in pixel (px) (983.28993)
20. distA_right_side_cm - Calculated distance of a line perpendicular to the line_1_right_side and its intersection of line_2_right_side in cm (2.08130)
21. distB_right_side - Calculated distance of a line perpendicular to the line_2_right_side and its intersection of line_1_right_side in pixel (px) (983.57903)
22. distB_right_side_cm - Calculated distance of a line perpendicular to the line_2_right_side and its intersection of line_1_right_side in cm (2.08191)
23. distAB_right_side_avg - Average of distA_right_side and distB_right_side in pixel (px) (983.43448)
24. distAB_right_side_avg_cm - Average of distA_right_side_cm and distB_right_side_cm in cm (2.08160)
25. calc_dist_left_side - Calculated distance between the the points defined by avg_right_side_A_x, avg_right_side_A_y and avg_right_side_B_x, avg_right_side_B_y in pixel (px) (981.34574)
26. calc_dist_left_side - Calculated distance between the the points defined by avg_right_side_A_x, avg_right_side_A_y and avg_right_side_B_x, avg_right_side_B_y in cm (2.07718)
27. avg_left_side_A_x - Analogue to avg_right_side_A_x but for the left side of the specimen (690.45745)
28. avg_left_side_A_y - Analogue to avg_right_side_A_y but for the left side of the specimen (1399.79787)
29. avg_left_side_B_x - Analogue to avg_right_side_B_x but for the left side of the specimen (606.27723)

30. avg_left_side_B_y - Analogue to avg_right_side_B_y but for the left side of the specimen (422.06931)
31. line_1_left_side - Analogue to line_1_right_side but for the left side of the specimen (-0.04133 + 1428.33131)
32. line_2_left_side - Analogue to line_1_right_side but for the left side of the specimen (-0.04113 + 447.00702)
33. distA_left_side - Analogue to distA_right_side but for the left side of the specimen (980.37059)
34. distA_left_side_cm - Analogue to distA_right_side_cm but for the left side of the specimen (2.07512)
35. distB_left_side - Analogue to distB_right_side but for the left side of the specimen (980.36215)
36. distB_left_side_cm - Analogue to distB_right_side_cm but for the left side of the specimen (2.07510)
37. distAB_left_side_avg - Analogue to distAB_right_side_avg but for the left side of the specimen (980.36637)
38. distAB_left_side_avg_cm - Analogue to distAB_left_side_avg_cm but for the left side of the specimen (2.07511)
39. calc_dist_length - Analogue to calc_dist_right_side but for the length of the specimen (7029.23297)
40. calc_dist_length_cm - Analogue to calc_dist_right_side_cm but for the length of the specimen (14.87854)
41. avg_length_A_x - Analogue to avg_right_side_A_x but for the length of the specimen (170.87179)
42. avg_length_A_y - Analogue to avg_right_side_A_y but for the length of the specimen (955.38462)
43. avg_length_B_x - Analogue to avg_right_side_B_x but for the length of the specimen (7192.50000)
44. avg_length_B_y - Analogue to avg_right_side_B_y but for the length of the specimen (628.50000)
45. line_1_length - Analogue to line_1_right_side but for the length of the specimen (-0.87051 + 1104.13027)
46. line_2_length - Analogue to line_2_right_side but for the length of the specimen (25.57616 + -183328.02318)
47. distA_length - Analogue to distA_right_side but for the length of the specimen (6963.98400)
48. distA_length_cm - Analogue to distA_right_side_cm but for the length of the specimen (14.74043)
49. distB_length - Analogue to distB_right_side but for the length of the specimen (11217.47002)
50. distB_length_cm - Analogue to distB_right_side_cm but for the length of the specimen (23.74364)
51. distAB_length_avg - Analogue to distAB_right_side_avg but for the length of the specimen (7029.23297)
52. distAB_length_avg_cm - Analogue to distAB_right_side_avg_cm but for the length of the specimen (14.87854)
53. calc_dist_center - Analogue to calc_dist_right_side but for the centre width of the specimen (541.39512)
54. calc_dist_center_cm - Analogue calc_dist_right_side_cm but for the centre width of the specimen (1.14595)
55. avg_center_A_x - Analogue to avg_right_side_A_x but for the centre width of the specimen (3675.02713)
56. avg_center_A_y - Analogue to avg_right_side_A_y but for the centre width of the specimen (1034.01938)
57. avg_center_B_x - Analogue to avg_right_side_B_x but for the centre width of the specimen (3783.48889)
58. avg_center_B_y - Analogue to avg_right_side_B_y but for the centre width of the specimen (503.60000)

59. line_1_center - Analogue to line_1_right_side but for the centre width of the specimen ($-0.04396 + 1195.57271$)
60. line_2_center - Analogue to line_2_right_side but for the centre width of the specimen ($-0.05674 + 718.26909$)
61. distA_center - Analogue to distA_right_side but for the centre width of the specimen (525.18692)
62. distA_center_cm - Analogue to distA_right_side_cm but for the centre width of the specimen (1.11165)
63. distB_center - Analogue to distB_right_side but for the centre width of the specimen (523.46612)
64. distB_center_cm - Analogue to distB_right_side_cm but for the centre width of the specimen (1.10800)
65. distAB_center_avg - Analogue to distAB_right_side_avg but for the centre width of the specimen (524.32652)
66. distAB_center_avg_cm - Analogue to distAB_right_side_avg_cm but for the centre width of the specimen (1.10982)
67. end_area_index - Index within the internal structure of found objects for software debugging (15)
68. angle_avg - The infill pattern detected in degrees. Detected by converting a portion around the centroid to binary and edge detection on the binarized image. The detected edges are averaged over all detected edges in the area of 120 pixel (px) height and width (41.50000)
69. rotated_rect_extent - Extent as described above but for the rotated bounding box, is always 1 (1.00000)
70. rotated_rect_len - The length of the rotated bounding box in px (16096.83508)
71. rotated_rect_area - The area of the rotated bounding box in square px (7036683.00000)
72. center_x - X Position of the center point (3682.09366)
73. center_y - Y Position of the center point (772.77529)
74. file - Full file name of scanned data (/mnt/experiment/sXX-67-opt.png)
75. corner_left_top - Position of the top-left corner as X and Y coordinates (176,449)
76. corner_right_top - Position of the top-left corner as X and Y coordinates (7168,158)
77. corner_left_bot - Position of the top-left corner as X and Y coordinates (211,1419)
78. corner_right_bot - Position of the top-left corner as X and Y coordinates (7197,1101)
79. top_distance_px - Calculated distance between the bottom corners in pixel (px) (6998.05294)
80. top_distance_cm - Calculated distance between the bottom corners in cm (14.81255)
81. bot_distance_px - Calculated distance between the bottom corners in pixel (px) (6993.23387)
82. bot_distance_cm - Calculated distance between the bottom corners in cm (14.80235)
83. elevation - Internal parameter of the enclosing ellipse, elevation of ellipse (-0.04162)
84. m_middle - Internal parameter of the enclosing ellipse (0.04357)
85. m_angle - Internal parameter of the enclosing ellipse (2.49471)
86. contour_perimeter - Length of the contour around the detected object in pixel (px) (17065.90852)
87. contour_perimeter_adj - Length of the contour around the detected object adjusted by the cm_factor to make it comparable among scanned files with differing resolution (36.12284)
88. extent - The extent of the detected object which is defined by the ratio of the contour area to the bounding box area (0.70249)
89. solid - The solidity of the detected object which is defined by the ratio of the contour area to its convex hull area (0.53456)
90. angle - Angle of the detected infill pattern (87.17921)
91. bounding_box(x, y, w, h) - X and Y position of the top left corner for the bounding box with the width and height of the bounding box (156, 125, 7057, 1301)
92. bounding_box_area_px - Area of the bounding box for the object in square cm (4907847.50000)
93. processing_time - Processing time for the geometry extraction in s (2.93760)

The following table (Table 6) lists all available objects contained in part B:

Table 6. Overview of contained specimen scans.

#	Page	Specimen #	Filename	Filesize in Bytes	Resolution in dpi	Image Width in Pixel (px)	Image Height in Pixel (px)
0	27	1	p27-1-1200.PNG	15,802,136	1200	7567	1495
1	27	1	p27-1-600.PNG	4,283,824	600	3685	759
2	27	2	p27-2-1200.PNG	16,257,137	1200	7429	1656
3	27	2	p27-2-600.PNG	4,213,422	600	3696	792
4	27	3	p27-3-1200.PNG	17,487,534	1200	7728	1725
5	27	3	p27-3-600.PNG	4,085,988	600	3596	768
6	27	4	p27-4-1200.PNG	18,594,572	1200	7429	1932
7	27	4	p27-4-600.PNG	3,425,931	600	3632	672
8	27	5	p27-5-1200.PNG	18,471,306	1200	7544	1863
9	27	5	p27-5-600.PNG	4,214,080	600	3632	804
10	27	6	p27-6-1200.PNG	15,456,270	1200	7452	1587
11	27	6	p27-6-600.PNG	3,405,681	600	3652	668
12	27	7	p27-7-1200.PNG	17,927,279	1200	7705	1725
13	27	7	p27-7-600.PNG	3,381,149	600	3628	672
14	28	10	p28-10-1200.PNG	18,385,665	1200	7613	1863
15	28	10	p28-10-600.PNG	3,795,305	600	3636	748
16	28	11	p28-11-1200.PNG	15,190,521	1200	7406	1541
17	28	11	p28-11-600.PNG	3,505,724	600	3646	660
18	28	12	p28-12-1200.PNG	15,950,936	1200	7291	1633
19	28	12	p28-12-600.PNG	3,426,744	600	3625	671
20	28	13	p28-13-1200.PNG	15,936,818	1200	7544	1587
21	28	13	p28-13-600.PNG	4,649,833	600	3624	852
22	28	14	p28-14-1200.PNG	16,473,597	1200	7636	1564
23	28	14	p28-14-600.PNG	3,950,749	600	3658	737
24	28	8	p28-8-1200.PNG	17,216,974	1200	7360	1794
25	28	8	p28-8-600.PNG	4,600,434	600	3773	858
26	28	9	p28-9-1200.PNG	16,645,140	1200	7590	1702
27	28	9	p28-9-600.PNG	33,88,757	600	3685	693
28	29	15	p29-15-1200.PNG	13,875,443	1200	7383	1449
29	29	16	p29-16-1200.PNG	15,349,450	1200	7475	1587
30	29	17	p29-17-1200.PNG	16,837,443	1200	7544	1725
31	29	18	p29-18-1200.PNG	15,908,333	1200	7406	1656
32	29	19	p29-19-1200.PNG	14,721,827	1200	7337	1541
33	29	20	p29-20-1200.PNG	16,315,248	1200	7452	1656
34	30	21	p30-21-1200.PNG	20,695,527	1200	7728	1978
35	30	22	p30-22-1200.PNG	17,279,097	1200	7475	1725
36	30	22	p30-22-600.PNG	4,152,746	600	3795	792
37	30	23	p30-23-1200.PNG	17,717,957	1200	7475	1748
38	30	24	p30-24-1200.PNG	15,798,242	1200	7636	1518
39	30	25	p30-25-1200.PNG	15,247,463	1200	7268	1541

Table 6. Cont.

#	Page	Specimen #	Filename	Filesize in Bytes	Resolution in dpi	Image Width in Pixel (px)	Image Height in Pixel (px)
40	30	26	p30-26-1200.PNG	15,821,651	1200	7452	1541
41	30	27	p30-27-1200.PNG	16,893,003	1200	7567	1587
42	31	28	p31-28-1200.PNG	12,403,406	1200	7326	1320
43	31	29	p31-29-1200.PNG	13,687,842	1200	7326	1430
44	31	31	p31-31-1200.PNG	13,380,146	1200	7238	1419
45	31	32	p31-32-1200.PNG	15,916,530	1200	7194	1672
46	32	36	p32-36-1200.PNG	22,134,196	1200	7728	2185
47	32	39	p32-39-1200.PNG	16,769,168	1200	7567	1702
48	34	47	p34-47-1200.PNG	17,601,188	1200	7475	1725
49	34	47	p34-47-600.PNG	4,951,121	600	3718	825
50	34	48	p34-48-1200.PNG	19,140,905	1200	7567	1886
51	34	48	p34-48-600.PNG	5,254,171	600	3740	814
52	34	49	p34-49-1200.PNG	14,877,228	1200	7337	1541
53	34	49	p34-49-600.PNG	4,659,681	600	3674	759
54	34	50	p34-50-1200.PNG	15,902,008	1200	7797	1541
55	34	50	p34-50-600.PNG	4,940,355	600	3795	781
56	34	51	p34-51-1200.PNG	18,265,770	1200	7498	1817
57	34	51	p34-51-600.PNG	5,664,148	600	3685	891
58	35	52	p35-52-1200.PNG	17,277,241	1200	7314	1794
59	35	53	p35-53-1200.PNG	16,928,700	1200	7291	1725
60	35	54	p35-54-1200.PNG	17,813,955	1200	7521	1771
61	35	55	p35-55-1200.PNG	15,224,841	1200	7406	1587
62	35	56	p35-56-1200.PNG	14,129,557	1200	7314	1495
63	35	57	p35-57-1200.PNG	14,474,452	1200	7498	1472
64	36	59	p36-59-1200.PNG	15,888,111	1200	8248	1616
65	36	60	p36-60-1200.PNG	12,207,369	1200	7264	1416
66	36	61	p36-61-1200.PNG	12,231,145	1200	7216	1400
67	36	62	p36-62-1200.PNG	11,898,430	1200	7248	1376
68	36	63	p36-63-1200.PNG	10,812,265	1200	7208	1248
69	36	64	p36-64-1200.PNG	13,461,738	1200	7336	1528
70	36	65	p36-65-1200.PNG	13,101,484	1200	7304	1474
71	36	66	p36-66-1200.PNG	12,640,867	1200	7370	1386
72	36	67	p36-67-1200.PNG	18,234,875	1200	7440	1648
73	36-b	58	p36-b-58-2400.PNG	51,724,257	2400	14760	2925
74	36-b	58	p36-b-58-4800.PNG	25,5270,856	4800	29520	5850
75	36-b	58	p36-b-58-600.PNG	764,250	600	3768	792
76	36-b	68	p36-b-68-2400.PNG	58,277,245	2400	15165	3195
77	36-b	68	p36-b-68-4800.PNG	289,659,569	4800	30330	6390
78	36-b	68	p36-b-68-600.PNG	969,708	600	3736	720
79	36-b	69	p36-b-69-2400.PNG	61,167,921	2400	15120	3375

Table 6. Cont.

#	Page	Specimen #	Filename	Filesize in Bytes	Resolution in dpi	Image Width in Pixel (px)	Image Height in Pixel (px)
80	36-b	69	p36-b-69-4800.PNG	121,977,342	4800	30240	6750
81	36-b	69	p36-b-69-600.PNG	1,002,549	600	3720	784
82	36-b	70	p36-b-70-2400.PNG	57,790,560	2400	14715	3240
84	36-b	70	p36-b-70-600.PNG	1,418,770	600	3696	784
85	36-b	71	p36-b-71-2400.PNG	70,141,930	2400	15165	3870
87	36-b	71	p36-b-71-600.PNG	903,541	600	3760	856
88	36-b	74	p36-b-74-2400.PNG	65,731,968	2400	15165	3555
90	36-b	74	p36-b-74-600.PNG	694,650	600	3704	800
91	37	75	p37-75-1200.PNG	16,789,946	1200	7521	1748
92	37	76	p37-76-1200.PNG	17,901,974	1200	7567	1886
93	37	77	p37-77-1200.PNG	13,748,061	1200	7383	1541
94	37	78	p37-78-1200.PNG	13,234,855	1200	7344	1488
95	37	79	p37-79-1200.PNG	13,518,732	1200	7408	1504
96	37	80	p37-80-1200.PNG	12,801,393	1200	7280	1440
97	37	81	p37-81-1200.PNG	13,856,233	1200	7344	1536
98	39	82	p39-82-1200.PNG	12,347,713	1200	7336	1360
99	39	83	p39-83-1200.PNG	11,992,064	1200	7288	1336
100	39	84	p39-84-1200.PNG	12,403,777	1200	7304	1392
101	39	85	p39-85-1200.PNG	12,825,914	1200	7376	1432
102	39	86	p39-86-1200.PNG	11,931,825	1200	7248	1352
103	39	87	p39-87-1200.PNG	12,522,546	1200	7168	1432
104	39	88	p39-88-1200.PNG	12,947,536	1200	7296	1440
105	40	89	p40-89-1200.PNG	15,188,761	1200	7498	1633
106	40	89	p40-89-2400.PNG	256,951,082	2400	15180	3496
107	40	90	p40-90-1200.PNG	14,157,006	1200	7282	1584
108	40	90	p40-90-2400.PNG	251,947,008	2400	14904	3496
109	40	91	p40-91-1200.PNG	14,281,697	1200	7260	1617
110	40	91	p40-91-2400.PNG	216,170,177	2400	14950	2990
111	40	92	p40-92-1200.PNG	13,946,621	1200	7249	1573
112	40	92	p40-92-2400.PNG	253,921,221	2400	15226	3450
113	40	93	p40-93-1200.PNG	13,320,929	1200	7238	1507
114	40	93	p40-93-2400.PNG	218,252,498	2400	14858	3036
115	40	94	p40-94-1200.PNG	14,266,965	1200	7293	1617
116	40	94	p40-94-2400.PNG	235,251,629	2400	14904	3266
117	40	95	p40-95-1200.PNG	14,442,902	1200	7348	1584
118	40	95	p40-95-2400.PNG	219,781,430	2400	14950	3036
119	41	100	p41-100-1200.PNG	13,213,145	1200	7370	1463
120	41	101	p41-101-1200.PNG	13,323,247	1200	7326	1474
121	41	102	p41-102-1200.PNG	13,527,017	1200	7315	1441

Table 6. Cont.

#	Page	Specimen #	Filename	Filesize in Bytes	Resolution in dpi	Image Width in Pixel (px)	Image Height in Pixel (px)
122	41	96	p41-96-1200.PNG	16,063,579	1200	7452	1771
123	41	97	p41-97-1200.PNG	16,517,917	1200	7429	1840
124	41	98	p41-98-1200.PNG	15,756,626	1200	7498	1748
125	41	99	p41-99-1200.PNG	14,660,149	1200	7406	1633
126	42	108	p42-108-2400.PNG	53,718,608	2400	14938	2992
127	42	109	p42-109-2400.PNG	54,466,318	2400	14894	3058
128	42	110	p42-110-2400.PNG	50,484,992	2400	14762	2860
129	42	111	p42-111-2400.PNG	56,011,807	2400	14586	3234
130	42	114	p42-114-2400.PNG	51,721,723	2400	14938	2926
131	42	117	p42-117-2400.PNG	48,238,820	2400	14718	2750
132	42	118	p42-118-2400.PNG	52,439,840	2400	14894	2948
133	42-a	104	p42-a-104-1200.PNG	15,651,976	1200	7314	1656
134	42-a	105	p42-a-105-1200.PNG	12,558,931	1200	7326	1397
135	42-a	106	p42-a-106-1200.PNG	14,685,907	1200	7337	1584
136	42-a	107	p42-a-107-1200.PNG	14,410,532	1200	7381	1540
137	43	119	p43-119-1200.PNG	15,112,558	1200	7360	1648
138	43	119	p43-119-2400.PNG	65,666,516	2400	14940	3690
139	43	119	p43-119-600.PNG	4,507,979	600	3850	869
140	43	120	p43-120-1200.PNG	13,527,108	1200	7288	1488
141	43	120	p43-120-2400.PNG	56,249,982	2400	14940	3150
142	43	120	p43-120-600.PNG	4,344,477	600	3696	880
143	43	121	p43-121-1200.PNG	12,108,927	1200	7288	1320
144	43	121	p43-121-2400.PNG	58,926,508	2400	14850	3330
145	43	121	p43-121-600.PNG	4,367,353	600	3773	869
146	43	122	p43-122-1200.PNG	12,052,518	1200	7392	1304
147	43	122	p43-122-2400.PNG	59,192,015	2400	14940	3330
148	43	122	p43-122-600.PNG	4,066,311	600	3729	814
149	43	124	p43-124-1200.PNG	13,076,273	1200	7280	1432
150	43	124	p43-124-2400.PNG	58,627,856	2400	15120	3240
151	43	124	p43-124-600.PNG	3,966,950	600	3718	803
152	43	126	p43-126-1200.PNG	13,476,698	1200	7320	1464
153	43	126	p43-126-2400.PNG	52,758,176	2400	14940	2925
154	43	126	p43-126-600.PNG	3,863,005	600	3795	759
155	43	127	p43-127-1200.PNG	12,857,843	1200	7328	1392
156	43	127	p43-127-2400.PNG	52,801,769	2400	14760	2970
157	43	127	p43-127-600.PNG	3,859,578	600	3751	770
158	45	142	p45-142-1200.PNG	16,394,947	1200	7544	1725
159	45	143	p45-143-1200.PNG	15,123,653	1200	7544	1587

Table 6. Cont.

#	Page	Specimen #	Filename	Filesize in Bytes	Resolution in dpi	Image Width in Pixel (px)	Image Height in Pixel (px)
160	45	144	p45-144-1200.PNG	15,093,669	1200	7498	1610
161	45	145	p45-145-1200.PNG	15,131,686	1200	7475	1610
162	45	146	p45-146-1200.PNG	15,904,074	1200	7659	1656
163	45	147	p45-147-1200.PNG	15,752,037	1200	7590	1656
164	45	148	p45-148-1200.PNG	16,846,784	1200	7613	1748
165	46	149	p46-149-1200.PNG	15,574,132	1200	7613	1610
166	46	150	p46-150-1200.PNG	15,281,620	1200	7590	1587
167	47	151	p47-151-1200.PNG	16,877,101	1200	7337	1863
168	47	152	p47-152-1200.PNG	14,001,437	1200	7491	1507
169	47	155	p47-155-1200.PNG	16,294,742	1200	7535	1716
170	50	171	p50-171-1200.PNG	16,061,329	1200	7498	1679
171	50	171	p50-171-2400.PNG	15,126,063	2400	15712	3583
172	50	173	p50-173-1200.PNG	15,414,649	1200	7498	1633
173	50	173	p50-173-2400.PNG	21,872,017	2400	15200	3144
174	50	176	p50-176-1200.PNG	15,237,904	1200	7475	1610
175	50	176	p50-176-2400.PNG	20,824,114	2400	14768	3144
176	50	180	p50-180-1200.PNG	13,818,923	1200	7498	1449
177	50	180	p50-180-2400.PNG	21,686,585	2400	15344	3071
178	50	181	p50-181-1200.PNG	15,041,539	1200	7774	1518
179	50	181	p50-181-2400.PNG	22,589,243	2400	15488	2925
180	51	182	p51-182-1200.PNG	16,710,584	1200	7475	1771
181	51	182	p51-182-2400.PNG	25,453,500	2400	15280	3144
182	51	183	p51-183-1200.PNG	15,383,101	1200	7475	1633
183	51	183	p51-183-2400.PNG	25,004,238	2400	15344	3144
184	51	183	p51-183-4800.PNG	82,642,045	4800	30848	6727
185	51	184	p51-184-1200.PNG	14,678,869	1200	7590	1541
186	51	184	p51-184-4800.PNG	72,257,123	4800	29536	5996
187	51	185	p51-185-1200.PNG	14,316,643	1200	7268	1518
188	51	185	p51-185-2400.PNG	29,494,201	2400	14976	3363
189	51	185	p51-185-4800.PNG	93,601,850	4800	29968	6727
190	52	186	p52-186-1200.PNG	13,571,583	1200	7314	1495
191	52	187	p52-187-1200.PNG	15,684,059	1200	7475	1725
192	52	188	p52-188-1200.PNG	21,223,550	1200	7521	2185

In part B there are 33 images with a resolution of 600 dpi, 116 at 1200 dpi, 35 at 2400 dpi and 6 images at 4800 dpi for a total of 193 images.

The average filesize and image properties are listed in the table below (Table 7):

Table 7. Average filesize in MiB, width and height in px of images in part B.

Resolution in dpi	Average filesize in MiB	Average Width in pixel (px)	Average Height in pixel (px)
600	3.4297	3705.1818	3728.5151
1200	14.4784	7433.7413	7452.5775
2400	80.9387	15011.2571	15107.3428
4800	97.0085	30059.1111	30806.5555

4. Summary

The dataset is compiled during research on the influence of object orientation and infill-orientation in FDM 3D-printing on the structural and geometrical quality of objects. The research is focused on the measurement and analysis of structural implications of varying infill orientations for which the flexural testing is performed, which is the focus of a separate publication. For the quality assessment the geometrical fidelity of the 3D-printer is analysed for which this dataset is used. The dataset is compiled over a period of three weeks in a office-environment to reflect the use-case of home-office usage. The dataset is of value to perform further geometrical analysis on the specimens, as well as to analyse error patterns and error modes with their physical reflection in FDM 3D-printing. The dataset are of use as an educational resource due to their high quality and allow for students to see the influence of the movement and structural parts of a 3D-printer on the surface quality of the 3D-printing objects.

5. Usage Notes

The dataset layout is described in Sections 3 and 7. The provided data can be used as examples to study the effects of the layer deposition and its inherent flaws such as smeared beads. The relevant geometrical information is available in the respective text files for the scanned specimens as described in the scheme. The data is released under the CC-BY license and can be used according its terms.

6. Concluding Remarks

The experiment conducted on the mechanical properties of varying infill pattern is still in progress and the experiment on the geometrical properties will be published in an article by the title “Geometrical Fidelity of Consumer Grade 3D Printers” in Computer Aided Design & Applications, 2017 [37]. The authors are of the opinion that the underlying data set described in this work is beneficial to other researches and warrants publication of the dataset itself. The data set can be used to study movement and material deposition of FDM 3D-printers and their common faults and errors. From the dataset the repeatability of identical 3D-printed models can be studied. Furthermore, we think that the image data is valuable for teaching purposes on the FDM 3D-printing process.

7. Dataset Availability

The dataset is not previously published in any other location but with this article. In the dataset the following items (part A) are present as indicated in Table 8 with the page number indicated in the first column, the lowest item number and the highest item number in the following columns. Missing pages and pages indicated with letters are due to enumeration mistakes on the paper form, missing parts are due to 3D-printing errors rendering them unsuitable for scanning.

Table 8. Available pages and the respective specimens contained within.

Page	Lowest Item Number	Highest Item Number
27	1	7
28	8	14
29	15	20
30	21	27
31	28	33
32	36	39
34	47	51
35	52	57
36	59	67
36-b	58	74
37	75	81
39	82	88
40	89	95
41	96	102
42-a	104	107
42	108	118
43	119	127
45	142	148
46	149	150
47	151	155
50	171	181
51	182	185
52	186	188

Acknowledgments: We would like to thank David Correa for the design of the objects for this experiment and the renderings used withing this document.

Author Contributions: Felix Baumann, Julian Eichhoff and Dieter Roller conceived and designed the experiments; Felix Baumann performed the experiments; Felix Baumann analyzed the data; Felix Baumann wrote the software and paper; Julian Eichhoff and Dieter Roller performed proof-reading and feedback on the paper.

Conflicts of Interest: The authors declare no conflict of interest.

Abbreviations

The following abbreviations are used in this manuscript:

3DP	3D Printing (Technology)
ABS	Acrylonitrile butadiene styrene
AM	Additive Manufacturing
AMF	Advance Manufacturing Format
CIS	Contact Image Sensor
CT	Computer Tomography
DPI	Dots per Inch
FDM	Fused Deposition Modeling
FFF	Fused Filament Fabrication
HSV	Hue-Saturation-Value (Color Coding)
LOM	Laminated Object Modeling
LZW	Lempel-Ziv-Welch (Algorithm)
MiB	Mebibyte
PLA	Polylactic Acid
PNG	Portable Network Graphics (File Format)

RGB	Red-Green-Blue (Color Coding)
RM	Rapid Manufacturing
RP	Rapid Prototyping
RT	Rapid Tooling
SLA	Stereolithography
SLM	Selective Laser Melting
SLS	Selective Laser Sintering
STL	Stereolithography (File Format)
TIFF	Tagged Image File Format
px	Pixel

References

- Gibson, I.; Rosen, D.; Stucker, B. *Additive Manufacturing Technologies*, 2nd ed.; Springer: New York, NY, USA, 2015.
- Wong, K.V.; Hernandez, A. A Review of Additive Manufacturing. *ISRN Mech. Eng.* **2012**, *2012*, 1–10.
- Turner, B.N.; Strong, R.; Gold, S.A. A review of melt extrusion additive manufacturing processes: I. Process design and modeling. *Rapid Prototyp. J.* **2014**, *20*, 192–204.
- Mohamed, O.A.; Masood, S.H.; Bhowmik, J.L. Optimization of fused deposition modeling process parameters: A review of current research and future prospects. *Adv. Manuf.* **2015**, *3*, 42–53.
- ISO. 6983-1:2009 *Automation Systems and Integration—Numerical Control of Machines—Program Format and Definitions of Address Words*; International Organization for Standardization: Geneva, Switzerland, 2009.
- ASTM ISO. *ASTM52915-13, Standard Specification for Additive Manufacturing File Format (AMF) Version 1.1*; ASTM International: West Conshohocken, PA, USA, 2013.
- Baumann, F.; Roller, D. 3D Printing Process Pipeline on the Internet. In Proceedings of the 8th ZEUS Workshop, Vienna, Austria, 27–28 January 2016; pp. 29–36.
- Bonten, C. *Kunststofftechnik*; Carl Hanser Verlag GmbH & Co. KG: Munich, Germany, 2014.
- Núñez, P.J.; Rivas, A.; García-Plaza, E.; Beamud, E.; Sanz-Lobera, A. Dimensional and Surface Texture Characterization in Fused Deposition Modelling (FDM) with ABS plus—In MESIC Manufacturing Engineering Society International Conference 2015. *Procedia Eng.* **2015**, *132*, 856–863.
- Baumann, F.; Schön, M.; Roller, D. Concept Development of a Sensor Array for 3D Printer. In Proceeding of the 3rd International Conference on Ramp Up Management (ICRM 2016), Aachen, Germany, 22–24 June 2016.
- Ippolito, R.; Iuliano, L.; Gatto, A. Benchmarking of Rapid Prototyping Techniques in Terms of Dimensional Accuracy and Surface Finish. *CIRP Ann.-Manuf. Technol.* **1995**, *44*, 157–160.
- Fadel, G.M.; Kirschman, C. Accuracy issues in CAD to RP translations. *Rapid Prototyp. J.* **1996**, *2*, 4–17.
- Pham, D.T.; Gault, R.S. A comparison of rapid prototyping technologies. *Int. J. Mach. Tools Manuf.* **1998**, *38*, 1257–1287.
- Matta, A.K.; Raju, D.R.; Suman, K.N.S. The Integration of CAD/CAM and Rapid Prototyping in Product Development: A Review—In 4th International Conference on Materials Processing and Characterization. *Mater. Today Proc.* **2015**, *2*, 3438–3445.
- Bikas, H.; Stavropoulos, P.; Chryssolouris, G. Additive manufacturing methods and modelling approaches: A critical review. *Int. J. Adv. Manuf. Technol.* **2016**, *83*, 389–405.
- Boparai, K.S.; Singh, R.; Singh, H. Development of rapid tooling using fused deposition modeling: A review. *Rapid Prototyp. J.* **2016**, *22*, 281–299.
- Dimitrov, D.; van Wijck, W.; Schreve, K.; de Beer, N. Investigating the achievable accuracy of three dimensional printing. *Rapid Prototyp. J.* **2006**, *12*, 42–52.
- Turner, B.N.; Gold, S.A. A review of melt extrusion additive manufacturing processes: II. Materials, dimensional accuracy, and surface roughness. *Rapid Prototyp. J.* **2015**, *21*, 250–261.
- Boschetto, A.; Bottini, L. Accuracy prediction in fused deposition modeling. *Int. J. Adv. Manuf. Technol.* **2014**, *73*, 913–928.
- Armillotta, A. Assessment of surface quality on textured FDM prototypes. *Rapid Prototyp. J.* **2006**, *12*, 35–41.

21. Equbal, A.; Sood, A.K.; Mahapatra, S.S. Prediction of dimensional accuracy in fused deposition modelling: A fuzzy logic approach. *Int. J. Prod. Qual. Manag.* **2011**, *7*, 22–43.
22. Sahu, R.K.; Mahapatra, S.S.; Sood, A.K. A Study on Dimensional Accuracy of Fused Deposition Modeling (FDM) Processed Parts using Fuzzy Logic. *J. Manuf. Sci. Prod.* **2013**, *13*, 183–197.
23. Masood, S.H.; Morsi, Y.S.; Katatny, I.E. Evaluation and Validation of the Shape Accuracy of FDM Fabricated Medical Models. *Adv. Mater. Res.* **2010**, *83*, 275–280.
24. Tong, K.; Joshi, S.; Lehtihet, E.A. Error compensation for fused deposition modeling (FDM) machine by correcting slice files. *Rapid Prototyp. J.* **2008**, *14*, 4–14.
25. Boschetto, A.; Bottini, L. Design for manufacturing of surfaces to improve accuracy in Fused Deposition Modeling. *Rob. Comput.-Integr. Manuf.* **2016**, *37*, 103–114.
26. Garg, A.; Bhattacharya, A.; Batish, A. On Surface Finish and Dimensional Accuracy of FDM Parts after Cold Vapor Treatment. *Mater. Manuf. Process.* **2016**, *31*, 522–529.
27. MITUTOYO | Product Information. Available online: <https://www.mitutoyo.co.jp/eng/products/nogisu/hyojyun.html> (accessed on 20 January 2016).
28. Taylor Hobson–Surface Profilers | Surface Profilometer. Available online: <http://www.taylor-hobson.com> (accessed on 20 January 2016).
29. Canon CanoScan LiDE 90 – Canon Europe. Available online: www.canon-europe.com/support/consumer_products/products/scanners/lide_series/canoscan_lide_90.aspx (accessed on 20 January 2016).
30. LTF – Prodotti Trovati. Available online: http://www.ltf.it/en/prodotti_lista.php (accessed on 20 January 2016).
31. Technical Support for Picza LPX-250RE 3D Laser Scanner. Available online: http://support.rolanddga.com/_layouts/rolanddga/productdetail.aspx?pm=LPX-250 (accessed on 20 January 2016).
32. AG, C.Z. ZEISS Industrial Metrology Homepage. Available online: www.zeiss.com/metrology/home.html (accessed on 20 January 2016).
33. Nikon Metrology, I. Optical Comparators | Video & Microscope Measuring | Products | Nikon Metrology. Available online: <http://www.nikonmetrology.com/Products/Video-Microscope-Measuring/Optical-Comparators> (accessed on 20 January 2016).
34. ISO. *Information Technology–Computer Graphics and Image Processing–Portable Network Graphics (PNG): Functional Specification*; ISO ISO/IEC 15948:2004; International Organization for Standardization: Geneva, Switzerland, 2004.
35. Dheemanth, H.N. LZW Data Compression. *Am. J. Eng. Res.* **2014**, *3*, 22–26.
36. DIN EN ISO. 527-2:2012-06 – *Kunststoffe - Bestimmung der Zugeigenschaften - Teil 2: Prüfbedingungen für Form- und Extrusionsmassen (ISO 527-2:2012)*; ISO: Geneva, Switzerland, 2012. (In Germany)
37. Baumann, F.W.; Wellekötter, J.; Roller, D.; Bonten, C. Software-aided measurement of geometrical fidelity for 3D printed objects. *Comput.-Aid. Des. Appl.* **2016**, 1–12, doi:10.1080/16864360.2016.1257190.



© 2017 by the authors; licensee MDPI, Basel, Switzerland. This article is an open access article distributed under the terms and conditions of the Creative Commons Attribution (CC-BY) license (<http://creativecommons.org/licenses/by/4.0/>).